Reactive Nitrogen Distribution and Partitioning in the North American Troposphere and Lowermost Stratosphere

H. B. Singh[1], L. Salas[1], D. Herlth[1], R. Kolyer[1], E. Czech[1], M. Avery[2], J. H. Crawford[2], R. B. Pierce[2], G. W. Sachse[2], D. R. Blake[3], R. C. Cohen[4], J. Dibb[5], G. Huey[6], R. C. Hudman[7], S. Turquety[7], L. K. Emmons[8], F. Flocke[8], Y. Tang[9], G. R. Carmichael[9], L. W. Horowitz[10]

1. NASA Ames Research Center, Moffett Field, CA 94035
2. NASA Langley Research Center, Hampton, VA 23665
3. University of California, Irvine, CA 92717
4. University of California, Berkeley, CA 92717
5. University of New Hampshire, Durham, NH 03824
6. Georgia Institute of Technology, Atlanta, GA 30332
7. Harvard University, MA 02138
8. National Center for atmospheric Research, CO 80301
9. University of Iowa, IA 52242
10. NOAA Geophysical Fluid Dynamics Laboratory, Princeton, NJ 08542

Submitted to Journal of Geophysical Research--Atmospheres

INTEX-A Special Section, June 2006

Abstract. A comprehensive group of reactive nitrogen species (NO, NO_2, HNO_3, HO_2NO_2, PANs, alkyl nitrates, and aerosol-NO_3^-) were measured in the troposphere and lowermost stratosphere over North America and the Atlantic during July/August 2004 (INTEX-A) from the NASA DC-8 platform (0.1-12 km). Less reactive nitrogen species (HCN and CH_3CN), that are also unique tracers of biomass combustion, were also measured along with a host of other gaseous (CO, VOC, OVOC, halocarbon) and aerosol tracers. Clean background air as well as air with influences from biogenic emissions, anthropogenic pollution, biomass combustion, and stratosphere was sampled both over continental U. S., Atlantic and Pacific. The North American upper troposphere was found to be greatly influenced by both lightning NO_x and surface pollution lofted via convection and contained elevated concentrations of PAN, ozone, hydrocarbons, and NO_x. Under polluted conditions PAN was a dominant carrier of reactive nitrogen in the upper troposphere while nitric acid dominated in the lower troposphere. Peroxynitric acid (HO_2NO_2) was present in sizable concentrations always peaking at around 8 km. Aerosol nitrate appeared to be mostly contained in large soil based particles in the lower troposphere. Plumes from Alaskan fires contained large amounts of PAN and very little enhancement in ozone. Observational data suggest that lightning was a far greater contributor to NO_x in the upper troposphere than previously believed. NO_x and NO_y reservoir appeared to be in steady state only in the middle troposphere where NO_x/NO_y was independent of air mass age. A first comparison of observed data with simulations from four 3-D models shows significant differences between observations and models as well as among models. These uncertainties likely propagate themselves in satellites derived NO_x data. Observed data are interpreted to suggest that soil sinks of

HCN/CH_3CN are at best very small. We investigate the partitioning and interplay of the reactive nitrogen species within characteristic air masses and further examine their role in ozone formation.

1. Introduction

Reactive nitrogen species play a central role in the chemistry of the polluted and unpolluted atmosphere. They critically determine levels of ozone, acidity, and atmospheric oxidation potential [Crutzen, 1976; Singh et al., 2003a]. When deposited, they act as nutrients in terrestrial and marine ecosystems. The main known constituents of reactive nitrogen in the troposphere are NO, NO_2, peroxyacyl nitrates (PANs; $RC(O)OONO_2$), nitric acid (HNO_3), peroxynitric acid (HO_2NO_2), alkyl nitrates ($RONO_2$), and particulate nitrate (NO_3^-). Other minor constituents such as HONO, NO_3, and N_2O_5 are also present but are quickly decomposed in day-light [Wayne et al., 1991]. Similarly somewhat long-lived species such as HCN and CH_3CN (lifetime ≈ 6 months) are globally abundant products of biomass combustion [Singh et al., 2003b and references there in]. In most previous studies it has been possible to measure only a subset of these reactive nitrogen species and often the data have been limited to the lower troposphere. The Intercontinental Chemical Transport Experiment-A (INTEX-A) offered a unique opportunity to investigate the partitioning and distribution of reactive nitrogen species from the North American troposphere at a level of detail previously not possible.

INTEX-A was a major field campaign conducted principally over North America (NA) and the Atlantic in the summer of 2004 under an international consortium called ICARTT (International Consortium for Atmospheric Research on Transport and

Transformation). ICARTT effort was jointly organized by partners from U. S., Canada, United Kingdom, Germany, and France and its design and implementation was closely coordinated [Singh et al., this issue]. A comprehensive suite of reactive nitrogen constituents, ozone, hydrocarbons, aerosols, chemical tracers, and meteorological parameters were measured aboard the NASA DC-8 and partner aircrafts in the troposphere and the Lower Most Stratosphere (LMS). In this manuscript we mainly use observations from the DC-8 to describe the distribution and partitioning of measured odd nitrogen and its relationship with ozone under polluted and pristine conditions. Observational data are also compared with simulations from multiple models of transport and chemistry to assess our present knowledge of photochemical theory as well as sources and sinks of reactive nitrogen.

2. Measurements

The intensive observational phase of INTEX-A was carried out from July 1 to August 15, 2004 over NA. The NASA DC-8 conducted 18 science flights extending from the mid-Pacific to the mid-Atlantic and covered much of the troposphere (0-12 km). Most intensive sampling was done over the eastern United States in collaboration with the NOAA P-3 that operated below 7 km altitude. During this period the UK BAe146 (ceiling 10 km) and the German Falcon (ceiling 13 km) sampled air downwind of NA over the Atlantic Ocean. A map of the geographical extent covered during INTEX-A/ICARTT and a summary of individual flights as well as instrumentation is provided in the overview papers by Singh et al. (this issue). The meteorological description for the region and for each of the missions are described by Fuelberg et al. (this issue) who also

provided detailed 5-10 day back trajectories along DC-8 flight tracks for the entire INTEX-A mission.

The NASA DC-8 aircraft was equipped with several in-situ instruments measuring ozone, reactive nitrogen species, aerosol composition, and a variety of chemical tracers. Nitrogenated constituents measured aboard the NASA DC-8 included NO, NO_2, HNO_3, HO_2NO_2, PAN, PPN, alkyl nitrates, aerosol nitrate, HCN, and CH_3CN. NO_3 and N_2O_5, which are of importance in nighttime chemistry, were also measured on the NOAA P-3 [Brown, et al. 2003]. The methods used to measure these species have been previously published and are summarized in Singh et al. [this issue] and references there in. Simply stated, ozone was measured by NO/O_3 chemiluminescence, PANs by electron-capture gas-chromatography (GC), HO_2NO_2 by chemical Ionization Mass spectrometry, nitric acid by mist chamber/IC technique, aerosol nitrate by filter collection, hydrocarbons by grab sampling and subsequent GC-FID/MS analysis, NO_2 by a Laser-Induced-Fluorescence (LIF), NO by chemiluminescence, and nitriles by GC using a Reduction Gas Detector.

A fast response CIMS instrument on the NOAA P-3 [Flocke et al, 2005] measured PAN and PPN which were found to be linearly correlated ([PPN] = 0.11 [PAN]; $R^2 = 0.86$). We have used this expression for estimating PPN from PAN on the DC-8 when appropriate. We also note that the NO instrument on the DC-8 had limited sensitivity and was suitable for measuring mixing rations >70 ppt. NO calculated from NO_2 data (sensitivity ≈ 10 ppt) using a steady state box-model agreed well with measured values for NO>100 ppt [Crawford et al., this issue]. To obtain a uniform data set we have defined NO_x as sum of measured NO_2 and calculated NO. Additionally, Total

Peroxyacyl Nitrates and Total Alkyl Nitrates were also determined aboard the DC-8 via indirect methods employing a combination of thermal dissociation and LIF detection of NO_2 [Day et al., 2002].

3. Data Analysis and Models

Merged data files were created to time align species measured with varying time resolutions and these have been used in this study. We have also used a variety of chemical and meteorological filters for purposes of air mass characterization. The principal chemical filter used was based on CO mixing ratios. When CO data were unavailable, C_2H_6 or C_2H_2 observations, which tended to be linearly correlated with CO, were used to fill data gaps. Although INTEX-A data were principally obtained in the troposphere, stratospheric influences were frequently encountered. Two stratospherically influenced data subsets were created. These included a stringent subset (O_3>200 ppb; CO<60 ppb; and Z>7 km) used primarily for defining LMS composition. A somewhat looser definition (O_3>120 ppb; H_2O<100 ppm and Z>7 km) was employed to also remove mixed stratospheric/tropospheric influences from the tropospheric subset. This subset has been principally used for tropospheric characterization in this study. Tropospheric data were further divided into: (i) Clean background (CO: 60-90 ppb or C_2H_6: 250-600 ppt); (ii) Polluted air masses (CO: 90-240 ppb or C_2H_6: 600-3000 ppt); and (iii) Episodic (CO: >240 ppb or C_2H_6: >3000 ppt). Episodic influences generally involved identifiable plume encounters.

Figure 1a,b shows the atmospheric distribution of HCN and CO, tracers of biomass combustion and general pollution respectively, for these subsets. It is evident

from HCN profiles that Biomass Burning influences were present throughout the troposphere during all periods of pollution. High pollution events (Episodic) contained enhanced signatures of biomass combustion. Further, both HCN and CO profiles provide a reasonable description of what can be expected to be present in the clean background air from historical data in this season [Holloway et al., 2000; Zhao et al., 2002; Edwards et al., 2004]. Data were also segregated geographically to represent the Pacific, Atlantic, and Continental regions. Multiple tracers were used to identify specific plumes originating from forest fires, anthropogenic emissions, convection and lightning, and stratosphere.

Total reactive nitrogen (NO_y), although not specifically measured in this study, was defined as follows:

$$NO_v = NO + NO_2 + HNO_3 + PAN + PPN + HO_2NO_2 + \Sigma RONO_2 + NO_3^-$$

In several previous studies the extent to which aerosol nitrate was sampled as NO_y has not been accurately known [Miyazaki et al., 2005]. During INTEX-A, aerosol nitrate was a small fraction of the total NO_y and has been included. N_2O_5 and NO_3 concentrations were extremely low and contributed negligibly to NO_y during day and minimally (<0.1% for Z>1 km) at night [Brown et al., 2005].

The data collected during INTEX-A were compared with results from three global and one regional Chemical Transport Models (CTMs). The three global CTMs used in this study included GEOS-CHEM [Bey et al., 2001; Hudman et al., this issue], MOZART [Horowitz et al., 2003; Pfister et al., 2005], and RAQMS [Pierce et al., 2003;

this issue]. The global models had a 2˚x2.5˚ nominal resolution. The regional model STEM had finer resolution and derived its boundary conditions from the MOZART global model [Tang et al., 2004; this issue]. The meteorological and emission fields input into these models were determined independently by each group. The total global NO_x source in these models varied from 40 to 50 Tg N yr^{-1}. However, the distribution of these emissions varied according to the model. As an example, global lightning source of NO_x (Tg N yr^{-1}) in RAQMS, GEOS-CHEM, and MOZART was 3, 5, and 9 respectively. More details on these models and their simulation techniques are being published separately [Hudman et al., this issue; Pierce et al., this issue; Tang et al., this issue].

4. Results and Discussion.

4.1 Partitioning and Atmospheric Behavior of Reactive Nitrogen:

Figure 2a,b show the partitioning of reactive nitrogen in the troposphere and the mean vertical structure of O_3 and NO_v based on data collected in INTEX-A. Tables 1 provides additional statistical information on the vertical structure of selected reactive N and tracer species. Table 2 shows the breakdown of individual C_1-C_5 alkyl nitrates whose sum is presented in Figure 2a and Table 1 in altitude bins representing lower troposphere (LT), middle troposphere (MT) and upper troposphere (UT). Mixing ratio of Total Alkyl Nitrates (TANs), measured at altitudes below 4 km by their conversion to NO_2, was some 10 times larger than the sum of individually measured straight chain alkyl nitrates (Table 2). These measurements suggest that sizable mixing ratios of higher alkyl nitrates (e. g. isoprene nitrate) may be present in the U. S. continental boundary layer. In

much of this study we have only used the more specific and presumably more accurate observations of individual alkyl nitrates. It is evident from Figure 2a that although reactive nitrogen is principally emitted as NO, throughout much of the troposphere it largely exists in its secondary reservoir forms. The total column of NO_x in the troposphere constituted only about 15% of the NO_y. PAN and HNO_3 were the dominant odd nitrogen species, containing some 65% of NO_y, with PAN dominating in the UT and HNO_3 in the LT. A moderate fraction of Reactive N in the UT was also due to HO_2NO_2 which was directly measured for the first time in this mission (Kim et al., this issue). Gaseous and aerosol nitrates comprised a very small fraction (<5%) of the tropospheric NO_y reservoir. As stated earlier, unmeasured alkyl nitrates (e. g. isoprene nitrate) may contribute up to 10% to NO_y in the continental boundary layer. Unlike O_3 which increased monotonically (Figure 2b), NO_v showed a C-shaped profile with high concentrations near the surface and the UT.

NO_x was the dominant reactive N species in the UT (Figure 2a). Mean NO_x/NO_v ratios of 0.3-0.6 here exceeded by a factor of two or more those found in the polluted surface layer and values reported from the mid-latitude UT downwind of Asia [Singh et al., 1996; Kondo et al., 1997] and NA [Jaegle et al., 1998; Koike et al., 2000]. In these and other studies, C_2H_2/CO ratio has been extensively used as a qualitative measure of air mass age. Figure 3 shows a plot of the NO_{yi}/NO_v as a function of air mass age. Because of the relatively short lifetime of NO_x compared to the reservoir species, NO_x/NO_v is expected to decrease with air mass age. This is clearly found to be the case in the lower troposphere (Figure 3a) where the lifetime of NO_x is short (<0.5 days) and NO_x/NO_v decreased by a factor of 3 with age. In the middle troposphere (2-7 km), the NO_x/NO_v

ratio was both low (≈ 0.1) and nearly independent of air mass age. We believe that this is indicative of the existence of a steady state between the NO_y reservoir species and NO_x {PAN ←→ NO_2 + PA; HNO_3 + hν ←→ NO_2 + OH; HNO_3 + OH → NO_2 + O + H_2O}. These low NO_x/NO_y ratios are also seen in extremely aged air masses in the LT. Model calculations by Jaegle et al. [1998] suggest that a NO_x/NO_y ratio in steady state should be between 0.05-0.1.

The UT region (7-12 km) behaved completely differently with high NO_x/NO_y ratios that also increased as a function of age. This is only possible if fresh injections of NO_x are being made in the UT. Benzene (C_6H_6) is a hydrocarbon of surface origin with about a 7 day lifetime, slightly longer than NO_x. NO_x/C_6H_6 ratios of about 60 during convective conditions in the UT are significantly higher than the ratios of about 10 even under polluted conditions suggesting that lofting of surface NO_x by convection could not have contributed more than 20% to the UT NO_x. The increase with age is likely due to the moderately long life-time of NO_x in the UT (4-6 days) that allows accumulation of NO_x from lightning and convective sources [Jeker et al., 2000]. Unlike the middle troposphere, a steady state with NO_y reservoir species was not achieved in the UT.

The INTEX-A time frame saw wide spread lightning throughout central and eastern NA [Porter et al, this issue]. A gridded (11 km x 11 km) inventory of lightning flashes (cloud to ground) over the United States during the entire INTEX-A period showed 100-250 flashes nearly everywhere east of 110 ˚W with large regions of 500-1600 flash counts. Comparison with previous 6 years suggested that these lighting flash frequencies were slightly above average (≈10%) but fairly typical of the summer season.

Indeed lightning source over NA during INTEX-A may have been 4-8 times what was assumed in the models (0.4 TgN y^{-1}). Aicrafts add some 0.5 TgN y^{-1} to the UT globally [Brasseur et al., 1998]. We estimate that over NA these emissions (≈ 0.1 TgN y^{-1}) contribute less than 50 ppt to UT NO_x and make only a small contribution in comparison with lightning effects. As we shall see later (Figures 4 and 5) lower stratosphere contained much less NO_x than the UT and hence was a minimal contributor. Observations performed over NA in the spring during the SUCCESS campaign showed substantially lower NO_x/NO_y ratios in the UT (≈ 0.15) compared to INTEX-A (≈ 0.3) presumably due to the absence of significant lightning despite several deep convective events [Jaegle et al., 1998]. We believe that lightning was a major source of NO_x in the UT during the summer of 2004.

The response of PAN and HNO_3 to aging was unlike NO_x but similar throughout the troposphere. At all altitudes NO_y fraction of PAN and HNO_3 declined and increased respectively with air mass age. The net increase in HNO_3 with age closely approximated the decrease in PAN, consistent with the notion that PAN reservoir feeds into NO_x and subsequently HNO_3.

4.2 Distribution of Reactive Nitrogen:

4.2.1. Reactive Gaseous Nitrogen. Figure 4a-d shows the abundance of reactive N species under "characteristic" conditions in the troposphere and the LMS. Under "clean" or "near background" conditions (Figure 4a), PAN and NO_x were extremely low in the LT and HNO_3 dominated. PAN gradually increased with altitude and in the UT was nearly as abundant as HNO_3. NO_x mixing ratios increased rapidly above 6 km and

become dominant above 8 km. HO_2NO_2 was present in sizable mixing ratios in the UT peaking at about 8 km. It is thermally highly unstable and easily decomposed at temperatures below 7 km (τ < 3 hrs). Above 7 km, its loss is slower (τ = 8 hrs) mostly dictated by reaction with OH and photolysis. The maximum observed at about 8 km coincides with a region of minimum loss. At still higher altitudes the loss rate is nearly constant but production tends to decline. In the polluted subset (Figure 4b) nearly all concentrations were elevated and a C-shaped profile with large values in the UT and LT was evident for both NO_x and NO_v. A dramatic change could also be seen in PAN which was now significantly more abundant than HNO_3 at all altitudes above 4 km. HO_2NO_2 still peaked at 9 km but was nearly twice as abundant as under clean conditions largely due to the high NO_x as well as HO_x precursors available under these conditions (HO_2 + NO_2 -> HO_2NO_2). Under all conditions, the NO_x levels in the UT were larger than their surface values and could not be attributed to surface pollution alone. These were likely due to the co-occurrence of convection and lightning influences. Under episodic conditions (Figure 4c), involving extreme levels of pollution, NO_y was extremely high (4-6 ppb) and PAN continued to dominate over HNO_3 to even lower levels. High HO_2NO_2 levels of 100-200 ppt, comparable to NO_x, were seen within these plumes at moderately low altitudes. Aerosol nitrate was present at concentrations much larger than NO_x in these air masses. The LMS composition was dramatically different where HNO_3 and NO_x were the dominant species with rather low PAN (Figure 4d).

Figure 5a-c shows the transition from troposphere to LMS (O_3< 440 ppb) for a select group of species. The NO_x mixing ratios of some 200-300 ppt in the LMS should be compared with some 600-3000 ppt in the UT (Fig 4a, b). Similarly NO_x/NO_y ratio of

0.2 in the LMS can be compared with 0.6 at 12 km. Since NO_x levels in the troposphere continue to rise to the DC-8 ceiling altitude of 12 km, it is likely that a NO_x maximum above this altitude was present with levels subsequently decreasing towards the tropopause. Such high NO_x maximum coincident with lightning conditions have been previously observed at subtropical latitudes and over Europe [Huntrieser et al., 2002; Ridley et al., 2004]. In the LMS, NO_x and HCN levels remained relatively constant while PAN, CO, and H_2O declined and HNO_3 increased. This behavior was similar to what has been previously reported from other locations and seasons [Singh et al., 1997].

Figure 6a,b shows the mean vertical structure of NO_x and PAN from west to east over NA. Since only one flight over the Pacific was conducted during INTEX-A, it is likely biased due to the encounter of Asian pollution in the UT. To give a better perspective we have also shown the NO_x and PAN distribution over the Pacific observed during Trace-P with a somewhat better statistical sample but in spring 2001. It is evident that NO_x levels in the UT increase from west to east. Signatures of continental pollution were similarly seen. This is evident in the lower troposphere for PAN although less so in the UT in part due to the relatively long lifetime of PAN in this region. West to east gradients were also seen under clean conditions in part due to residual pollution influences and lightning effects. We note that CO showed no west to east gradient in the UT. Figure 7 shows the longitudinal variation in the upper troposphere (7-12 km) of O_3 and select reactive nitrogen species both under clean and actual observed conditions. Ozone mixing ratios in the UT were enhanced by 10-15 ppb (Figure 7a). This has also been observed from the ozonesonde data analyzed by Cooper et al. [this issue]. A much larger increase is seen in PAN which is an excellent indicator of pollution and

photochemical influences (Figure 7b). It is also evident from the NO_x profile that lightning and the associated convection had a big impact over central US (Figure 7c). Correspondingly, little change is seen in HNO_3 (Figure 7d), in part because of its high solubility and loss during wet convection. In short the North Ameican UT appears to be greatly influenced by pollution resulting in substantial enhancements in ozone, PAN, and tracers of pollution.

4.2.2 Aerosol Nitrogen. Aerosol nitrate can be typically formed via reaction of NH_3 and nitric acid ($NH_3 + HNO_3 <-> NH_4NO_3$). Total aerosol nitrate (NO_3^-) in INTEX-A was found to be moderately correlated with NH_4^+ (R^2=0.42) suggesting a chemical form such as NH_4NO_3. An examination of the NH_4^+ and SO_4^{--} ion balance (Figure 8a) clearly indicates that throughout INTEX-A excess sulfate was nearly always present suggesting insufficient ammonia for acid neutralization. This is unlike what was observed in the Asian pollution outflow where excess ammonium was present and all SO_4 had been neutralized [Miyazaki, et al., 2005]. Ammonia is preferentially converted to ammonium sulphate as long as SO_4^{--} is present [Seinfeld and Pandis, 1998], and indeed SO_4^{--} and NH_4^+ were highly correlated (R^2=0.85). We conclude that NH_4NO_3 was not the preferential form of the aerosol nitrate observed over NA. Figure 8b further shows that NO_3^- was well correlated with soil elements like calcium. As has been previously noted [Krueger et al., 2005], it appears that the source of this nitrate aerosol is HNO_3 residing on and reacting with soil and crustal particles which are typically of large size (e. g. $2HNO_3$ (g) + $CaCO_3$ (s) -> $Ca(NO_3)_2$ (s)+ H_2O + CO_2). This is further supported by the presence of extremely small measured concentrations of submicron NO_3^-. This form of

aerosol nitrate represents a somewhat permanent sink for reactive nitrogen eventually to be deposited on soil.

4.2.3 Plumes. By employing a number of selected tracers, characteristic plumes sampled during INTEX-A were segregated into categories representing influences from Biomass Burning (B), Anthropogenic pollution (P), Deep Convection (C), and Stratosphere (S). For example, HCN and CH_3CN were highly elevated in BB plumes and high O_3 and low CO and H_2O mixing ratios were characteristic of stratospheric influences. Figure 9 shows the distribution of selected species in these plumes as a function of altitude bins representing LT (0-2 km), MT (2-7 km), and UT (7-12 km). Foremost is the appearance of high PAN and relatively low NO_x in BB plumes (Figure 9a). Another distinct feature was the high NO_x mixing ratios observed in convectively influence plumes (Figure 9b). Despite the high NO_x values encountered in these convective plumes, O_3 was not significantly elevated (Figure 9c). Similarly O_3 was rather low in BB burning plumes as well. It has been estimated that most of these convective plumes were only 2-3 days old [Bertram et al., this issue], and there may have been insufficient time for significant O_3 production in the UT. Both HNO_3 and aerosol nitrate were significantly elevated in plumes influenced by anthropogenic and biomass burning pollution (Figure 9d). Law et al [this issue] have explored the development of some of these plumes over the Atlantic and conclude that net O_3 production does occur but is greatly slowed due to the control exerted by PAN on the NO_x reservoir.

4.2.4 Nitrogen Tracers of Biomass Combustion. HCN and CH_3CN are both unique tracers of BB combustion and were linearly correlated in this data set (R^2= 0.76). Figure 10 shows the vertical structure of HCN and CH_3CN over the Atlantic and continental NA. There is the indication of both oceanic and soil sink for these species. Although oceanic sink has been known, soil sink is not known and has not been studied. Figure 10 also shows similar profiles for $CHBr_3$ and CH_3I which are both known to have dominant oceanic sources. It is evident from Fig. 10 that at least in surface layers over land oceanic influences were widespread. To further explore the soil sink potential for nitriles we performed trajectory analysis and looked at their distribution for selected cases where trajectories remained low and over the ocean with those when they remained low and over land for 5 days. Overland air masses had mixing ratios of 260 (±20) ppt and 135 (±14) ppt for HCN and CH_3CN while over water trajectories had corresponding mixing ratios of 149 (±33) ppt and 109 (±18) ppt. In short air masses with long contact with surface water are far more depleted than those with contact with soil. Despite the appearance of a sink, we conclude that HCN and CH_3CN soil sinks are negligible or extremely small. This could be due to low contact time between these molecules and soil bacteria allowing rapid re-release of deposited nitriles. The column of HCN deduced from these measurements is in good agreement with that reported by Zhao et al. [2000] from ground based spectroscopic measurements over japan..

4.3. Model Simulations

Model output was generated from four selected models (GEOS-CHEM, RAQMS, MOZART and STEM) along the DC-8 flight tracks and the results were

directly comparable with observations. Figures 11-13 provide a comparison of observations and model simulations using a large grid over eastern NA (30-50˚N; 260-320˚E) where most intense aircraft sampling was performed during INTEX-A. Figure 11 shows observed and modeled mean mixing ratios of O_3 and NO_y and the corresponding variability. As is evident, the four models under consideration deviate from each other and the observations at all altitudes. STEM substantially over-predicts O_3 in the UT and NO_y in all of the troposphere. RAQMS has extremely low NO_y but over-predicts O_3 suggesting an unusually large stratospheric input. Models in general tended to predict lesser variability (Figure 11c,d) than observations in large part due to the their greater spatial averaging.

Figure 12 shows the same for NO_x, HNO_3. PAN and HO_2NO_2. It is evident that except in the case of STEM, NO_x is substantially underpredicted by all models in the UT. GEOS-CHEM improved its overall prediction by increasing the lightning source over NA by a factor of four [Hudman et al., this issue]. It has recently been suggested that cloud to cloud discharges may be a far greater source of NO_x than has traditionally been believed [Ridley et al., 2005]. Clearly an underestimation of lightning source and uncertainties in its distribution appears to be a common problem in these models. STEM also over predicts near surface NO_x levels and the associated HNO_3 by 50-100%. It appears that STEM is using an earlier emissions inventory that does not take into account the substantial emission reductions that have been achieved in the last 5 or so years. An intriguing aspect is that in the UT HNO_3 is typically over estimated while NO_x is underestimated. As has been seen elsewhere (Crawford et al., this issue), models are significantly over predicting OH (and HO_2) levels resulting in an over prediction in

HNO_3 (NO_2+OH → HNO_3). To simulate HNO_3 correctly a significant revision in the HO_x field would be necessary. The situation with PAN (and HO_2NO_2) is also confusing with significant over predictions by MOZART in the middle and upper troposphere and STEM in the LT. Figure 13 shows the distribution of total aerosol NO_3 and its simulation by two models. These models are able to simulate the UT or LT with reasonable accuracy but not both. While models have become more complex, it is not clear if the overall performance in simulating reactive nitrogen has improved over the last decade [Emmons et al., 1997; Thakur et al., 1999].

Our ability to simulate the reactive nitrogen fields and O_3 in the troposphere is less than satisfactory both for the NO_x and HO_x fields. Uncertainties are clearly due to errors in sources and meteorology but probably include fundamental limitations in our knowledge. Organized model inter-comparisons and more validation data are required to better pin point the causes of these uncertainties and potential solutions. In recent years, it has been possible to retrieve NO_x columns in the troposphere from satellite observations and these have been used to provide extensive data coverage as well as inferences of NO_x emissions (Richter et al., 2005; Heckel et al. 2006; Martin et al., 2006). Retrieval of satellite data requires a priory knowledge NO_x structure and the accuracy of retrievals is often dependent on this a priory knowledge. Traditionally model profiles have been used for this purpose. The NO_x observations from this study clearly show that the vertical structure of NO_x across the troposphere is highly complex and its extensive characterization necessary for accurate satellite retrievals.

5.0 Conclusions

INTEX-A provided a most detailed description of the reactive nitrogen, ozone, and tracer field in the North American tropsosphere. The observations clearly show that the UT as well as LT is significantly polluted across NA. The UT is also greatly influenced by deep convection and far greater lightning than hitherto believed. Only in the middle troposphere is NO_x in steady state maintained by the NO_y reservoir. NO_x/NO_y ratios are significantly more elevated in the UT than in the LT and support fresh injections of NO_x originating in the troposphere. PAN appears to be the major carrier of reactive nitrogen in the UT while much of it exists in the HNO_3 reservoir in the LT. Presently model simulations of these species cannot be performed satisfactorily as models disagree with each other as well as observations to a substantial degree. It is possible that in some cases disagreements in the reactive nitrogen simulations are due to uncertainties in the HO_x field. The causes of these disagreements are not fully understood and need to be further investigated. The vertical structure of NO_x over the continents is far more complex than represented by models making it extremely difficult for satellites to accurately retrieve NO_x data using remote sensing techniques. Extensive validations are necessary to improve models as well as satellite determinations of NO_x.

References:

Bey, I., et al., Global modeling of tropospheric chemistry with assimilated meteorology: Model description and evaluation, J. Geophys. Res., 106, 23,073–23,096, 2001.

Bertram, T.H., et al., Convection and the Age of Air in the Upper Troposphere, J. Geophys. Res., this issue.

Brasseur, G. P. et al., European scientific assessment of the atmospheric effects of aircraft emissions, Atmos. Environ., 32 (13), 2329-2418, 1998.

Brown, S. S., H. Stark, T. B. Ryerson, E. J. Williams, D. K. Nicks Jr., M. Trainer, F. C. Fehsenfeld, and A. R. Ravishankara, Nitrogen oxides in the nocturnal boundary layer: Simultaneous in situ measurements of NO_3, N_2O_5, NO_2, NO, and O_3, J. Geophys. Res., 108(D9), 4299, doi:10.1029/2002JD002917, 2003.

Brown, S. S. et al., Variability in nocturnal nitrogen oxide processing and its role in regional air quality, Fall AGU, A43F-02, 2005.

Cooper, O. R., et al., Large upper tropospheric ozone enhancements above mid-latitude North America during summer: In situ evidence from the IONS and MOZAIC ozone monitoring network, J. Geophys. Res., this issue.

Crawford, J., et al., Summertime ozone production over North America during INTEX-A based on observed and modelled photochemistry, J. Geophys. Res., this issue.

Crutzen, P.J., 1979. The role of NO and NO_2 in the chemistry of the troposphere and stratosphere. Annual Review of Earth and Planetary Sciences , 7, 443-472, 1979.

Day, D. A., P. J. Wooldridge, M. B. Dillon, J. A. Thornton, and R. C. Cohen, A thermal dissociation laser-induced fluorescence instrument for in situ detection of NO2,

peroxy nitrates, alkyl nitrates, and HNO_3, J. Geophys. Res., 107(D6), 4046, doi:10.1029/2001JD000779, 2002.

Edwards, D. P., et al., Observations of carbon monoxide and aerosols from the Terra satellite: Northern Hemisphere variability, J. Geophys. Res., 109, D24202, doi:10.1029/2004JD004727, 2004

Emmons, L.K. et al., Climatologies of NO*x* and NO*y*: a comparison of data and models. Atmos. Environ., 31, 1851-1904, 1997.

Flocke, E. et al., Results from fast airborne measurements of PANs during the 2004 New England Air Quality Study, Fall AGU, A54C-03, 2005.

Fuelberg, H. E., M. J. Porter, C. M. Kiley, D. Morse, The representativeness of meteorological conditions during INTEX-NA, J. Geophys. Res., this issue.

Heckel, A., et al., Validation of SCIAMACHY tropospheric NO_2 and HCHO columns during INTEX-A/ICARTT, J. Geophys. Res., this issue.

Holloway, T., H. Levy II, and P. Kasibhatla, Global distribution of carbon monoxide, J. Geophys. Res., 105(D10), 12,123–12,148, 2000.

Horowitz, L. W., A global simulation of tropospheric ozone and related tracers: description and evaluation of MOZART, version 2, J. Geophys. Res, 108 (D24), 4784, doi:10.1029/2002JD002853, 2003.

Hudman R.C., et al., A multi-platform analysis of the North American reactive nitrogen budget during the ICARTT summer intensive, J. Geophys. Res., this issue.

Huntrieser, H., et al., Airborne measurements of NO_x, tracer species, and small particles during the European lightning nitrogen oxides experiment. J. Geophys. Res, 107

(D11), 4113 (doi:10.1029/2000JD000209), 2002.

Jeker, D. P. , L. Pfister, A.M. Thompson, D. Brunner, D. Boccippio, K.E. Pickering, H. Wernli, Y. Kondo and J. Staehelin, Measurements of nitrogen oxides at the tropopause: attribution to convection and correlation with lightning. J. Geophys. Res 105 (D3), 3679–3700, 2000.

Jaegle, L., Jacob, D. J., Wang, Y., Weinheimer, A. J., Ridley, B. A., Campos, T. L., Sachse, G. W., and Hagen, D. E.: Sources and chemistry of NO_x in the upper troposphere over the United States, Geophys. Res. Lett., 25, 1705–1708, 1998.

Kim, S., et al., Measurement of HO_2NO_2 in the Upper Troposphere during ICARTT/INTEX-A, J. Geophys. Res., this issue.

Koike, M., et al., Impact of aircraft emissions on reactive nitrogen over the North Atlantic Flight Corridor region, J. Geophys. Res., 105 (D3), 3665–3677, 2000.

Kondo, Y., et al., Profiles and Partitioning of Reative Nitrogen Over the Pacific Ocean in Winter and Early Spring, J. Geophys. Res., 102, 28,405-28,424, 1997.

Krueger, B. J., V.H. Grassian, J.P. Cowin and A. Laskin, Heterogeneous chemistry of individual mineral dust particles from different dust source regions: the importance of particle mineralogy, Atmos. Environ., 38, 6253-6261, 2004.

Law, K. et al., Evidence for Long-Range Transport of North American Anthropogenic and Wildfire Emissions to Europe from Airborne and Ground Based Lidar Measurements during European ITOP (IGAC Lagrangian 2K4, ICARTT), Fall AGU, A41D-01, 2005.

Martin, R. V., et al., Evaluation of space-based constraints on nitrogen oxide emissions with regional aircraft measurements over and downwind of eastern North America, J. Geophys. Res, this issue.

Miyazaki, Y. et al., Contribution of particulate nitrate to airborne measurements of total reactive nitrogen, J. Geophys. Res., 110, D15304, doi:10.1029/2004JD005502, 2005.

Pfister G., P. G. Hess, L. K. Emmons, J.-F. Lamarque, C. Wiedinmyer, D. P. Edwards, G. Pétron, J. C. Gille, G. W. Sachse, Quantifying CO emissions from the 2004 Alaskan wildfires using MOPITT CO data, Geophys. Res. Lett., 32, L11809, doi:10.1029/2005GL022995, 2005.

Pierce, R. B. et al., Regional Air Quality Modeling System (RAQMS) predictions of the tropospheric ozone budget over east Asia, J. Geophys. Res, 108, D21, 8825, doi:10.1029/2002JD003176, 2003.

Pierce, R. B., et al., Chemical data assimilation based estimates of Continental US Ozone and Nitrogen budgets during INTEX-A, J. Geophys. Res., this issue.

Porter, M., H. et al., Assesing convective influence by utilizing cloud to ground lightning data and high resolution kinematic trajectories, J. Geophys. Res., this issue.

Richter, A. J. P. Burrows, H. Nü, C. Granier, U. Niemeier, Increase in tropospheric nitrogen dioxide over China observed from space, Nature, 437, 129-132, 2005.

Ridley, B., et al. (2004), Florida thunderstorms: A faucet of reactive nitrogen to the upper troposphere, J. Geophys. Res., 109, D17305, doi:10.1029/2004JD004769.

Ridley, B. A., K. E. Pickering, and J.E. Dye, Comments on the parameterization of lightning-produced NO in global chemistry-transport models, Atmos. Environ.,

39, 6184-6187, 2005.

Seinfeld, J. H. and S. N. Pandis, Atmospheric Chemistry and Physics, John Wiley and Sons, New York, 1998.

Singh, H. B. et al., Reactive nitrogen and ozone relationships over the western Pacific: distribution, partitioning and sources, J. Geophys. Res., 101, 1793-1808, 1996.

Singh, H. B., et al., Trace chemical measurements from the northern midlatitude lowermost stratosphere: distributions, correlations, and fate, Geophys. Res. Lett., 24, 127-130, 1997.

Singh, H. B., W. H. Brune, and J. H. Crawford, Reactive nitrogen and hydrogen in the global atmosphere: progress in measurements and theory, in Recent Advances in Atmospheric and Oceanic Sciences-Part-II: Air Pollution Studies, Proceedings of the Indian National Science Academy, 69/6, 669-683, 2003a.

Singh, H. B., et al., In situ measurements of HCN and CH_3CN over the Pacific Ocean: Sources, sinks, and budgets, J. Geophys. Res., 108(D20), 8795, doi:10.1029/2002JD003006, 2003b.

Singh, H. B., W. Brune, J. Crawford, and D. Jacob, Overview of the Summer 2004 Intercontinental Chemical Transport Experiment-North America (INTEX-A), J. Geophys. Res., this issue.

Tang, Y., et al., Three-dimensional simulations of inorganic aerosol distributions in East Asia during spring 2001, J. Geophys. Res., 109, D19S23, doi:10.1029/2003JD004201, 2004.

Tang, Y., et al., The influence of lateral and top boundary conditions on regional air quality prediction: a multi-scale study coupling regional and global chemical transport models, J. Geophys. Res., this issue.

Thakur, A. N., H. B. Singh, P. Mariani, Y. Chen, Y. Wang, D. Jacob, G. Brasseur, J-F. Muller and M. Lawrence, Distribution of Reactive Nitrogen Species in the Remote Free Troposphere: Data and Model Comparisons, Atmos. Environ, 33, 1403-1422, 1999.

Wayne, R. P., et al., The nitrate radical: physics, chemistry, and the atmosphere, Atmos. Environ. Part A, 25(1), 1–203, 1991.

Zhao Y., et al., Spectroscopic measurements of tropospheric CO, C_2H_6, C_2H_2, and HCN in northern Japan, J. Geophys. Res., 107 (D18), 4343, doi:10.1029/2001JD000748, 2002.

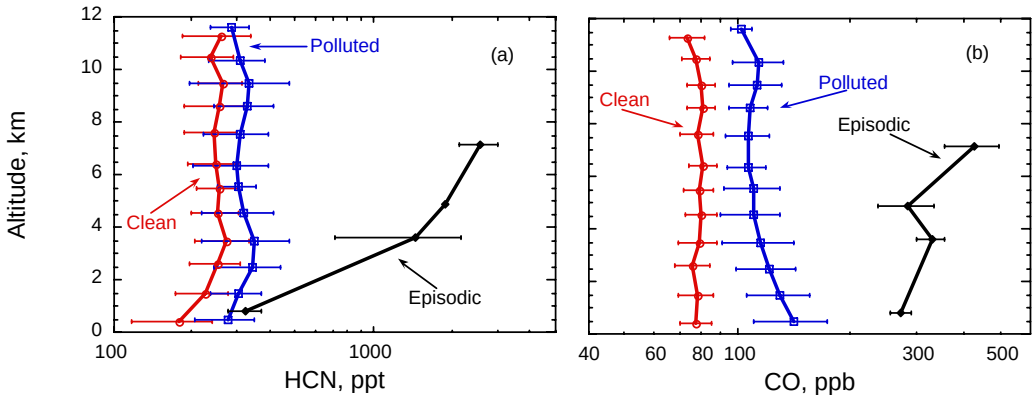

Figure 1: Distribution of two selected tracer species (HCN and CO) under "background", "polluted", and "episodic" conditions. See text for more detail.

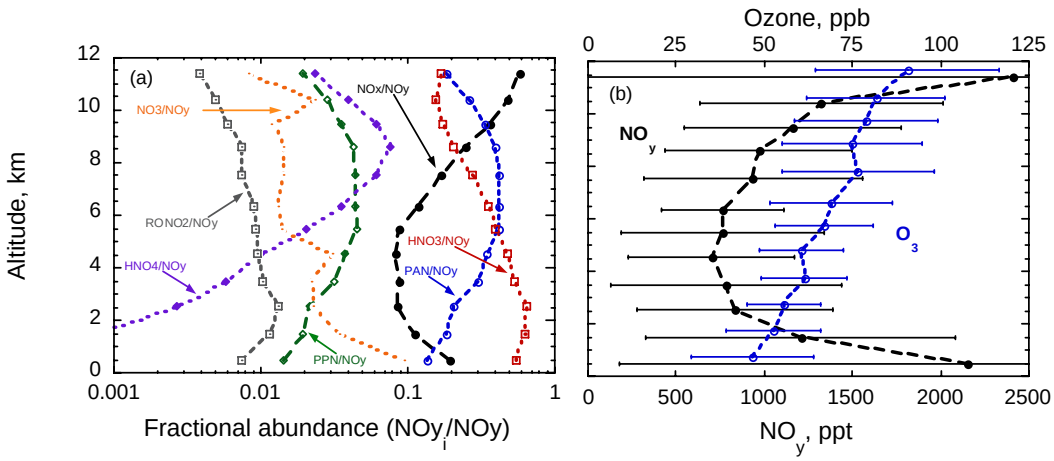

Figure 2: Partitioning of reactive nitrogen in the troposphere (a) and the mean vertical structure of O_3 and NO_y (b) based on INTEX-A observations

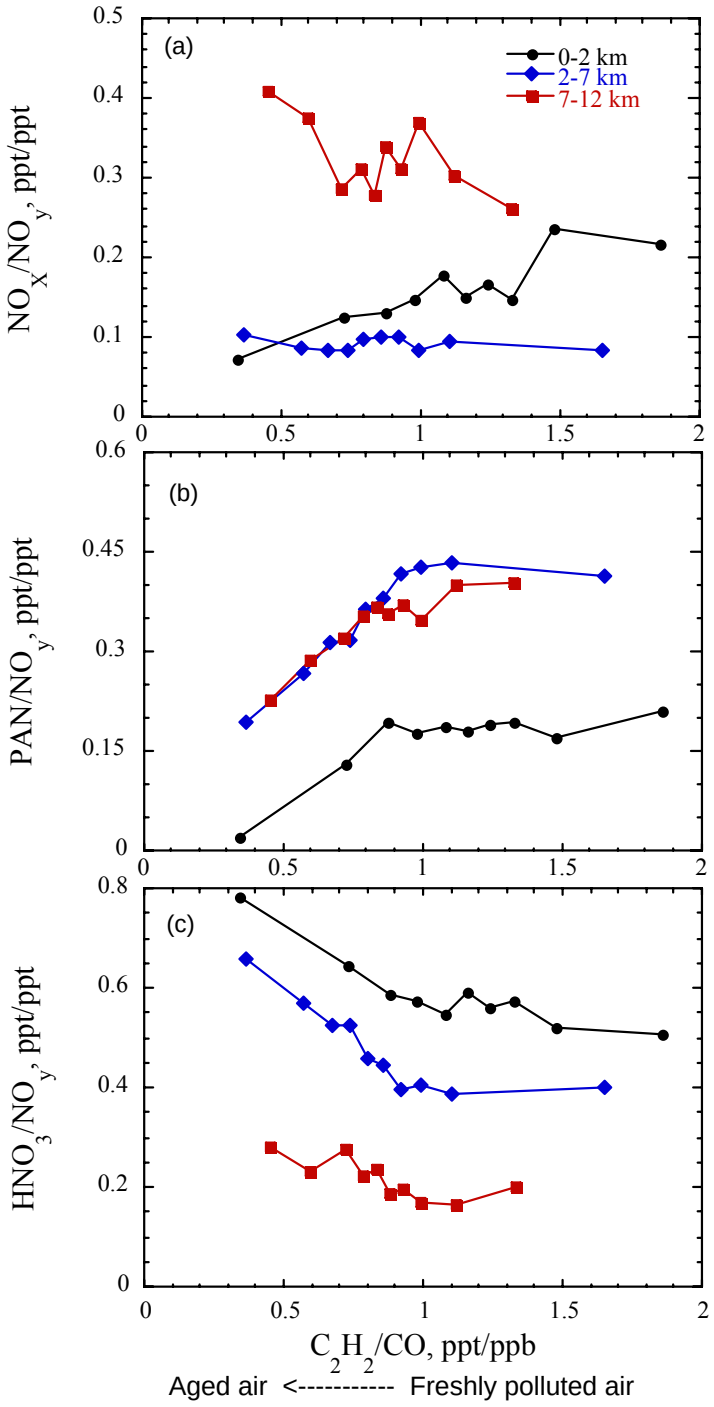

Figure 3: Reactive nitrogen as a function of air mass age in the lower (0-2 km), middle (2-7 km) and upper (7-12 km) troposphere (Lat: 30-50 ˚N; Long: 260-320 ˚E). All data were divided into 10 age bins. Each point shown above represents an average of 60-120 observed data points.

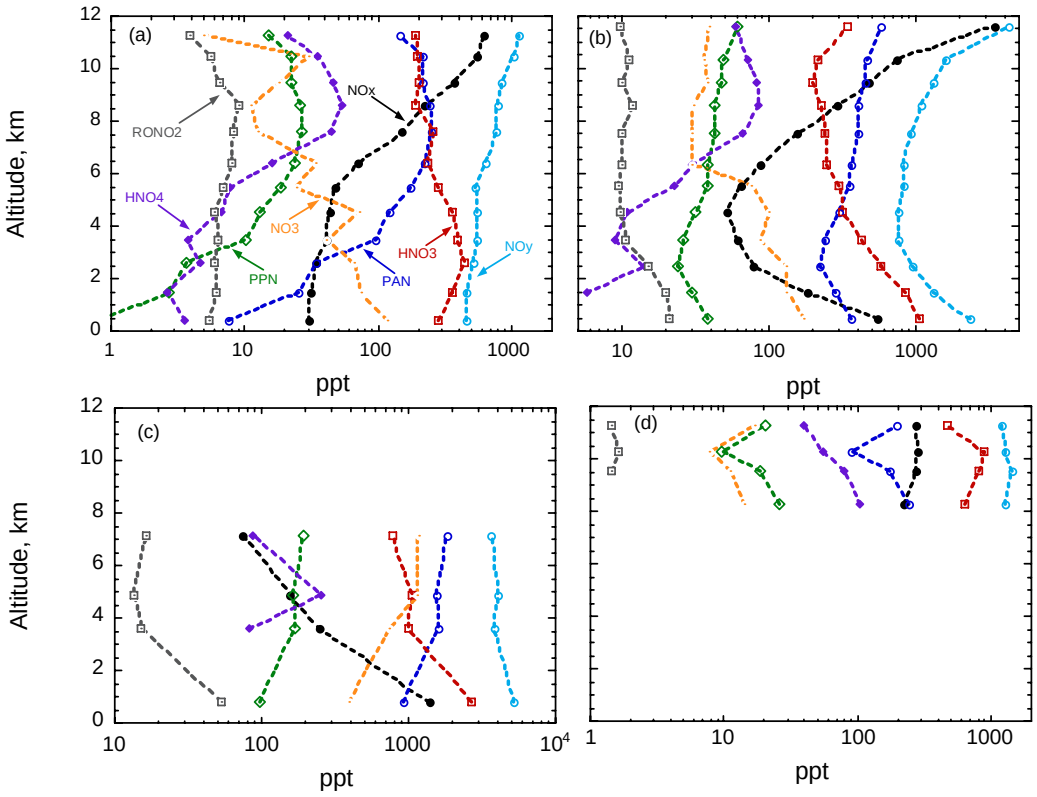

Figure 4: Reactive nitrogen species in the troposphere and Lower Most Stratosphere. (a) Background/clean; (b) Polluted; (c) Episodic; and (d) lowermost stratospheric. See text for more detail.

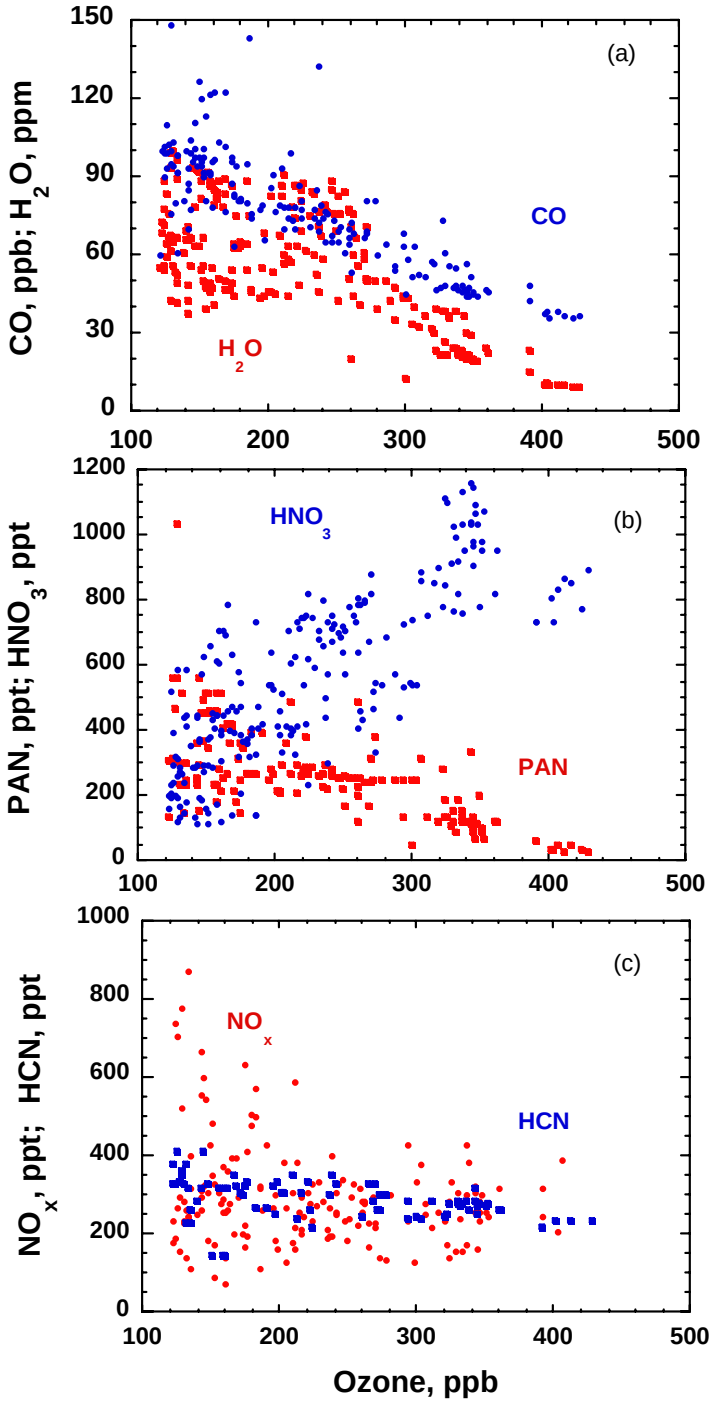

Figure 5: Mixing ratios of key tracers and reactive nitrogen species in the Lower Most Stratosphere sampled in INTEX-A

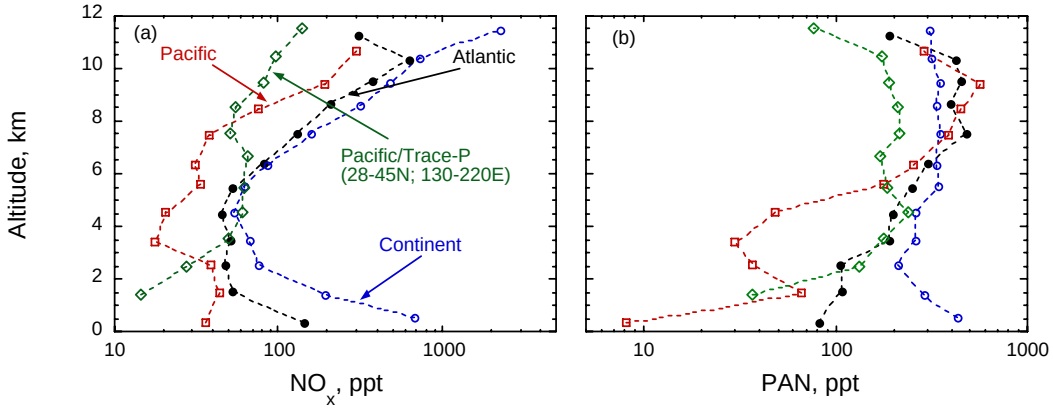

Figure 6: NO_x and PAN over the Pacific, continental North America, and the western Atlantic

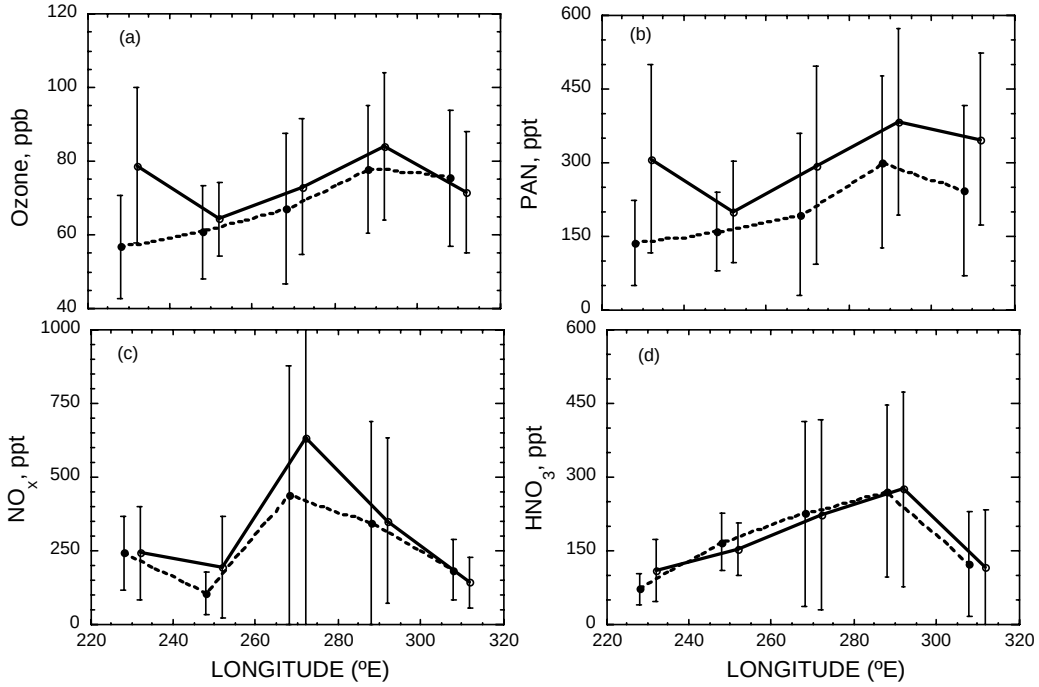

Figure 7: Ozone and reactive nitrogen in the North American upper troposphere (7-12 km; 30-45˚N)) under "background" (dashed) and all observed (solid) conditions

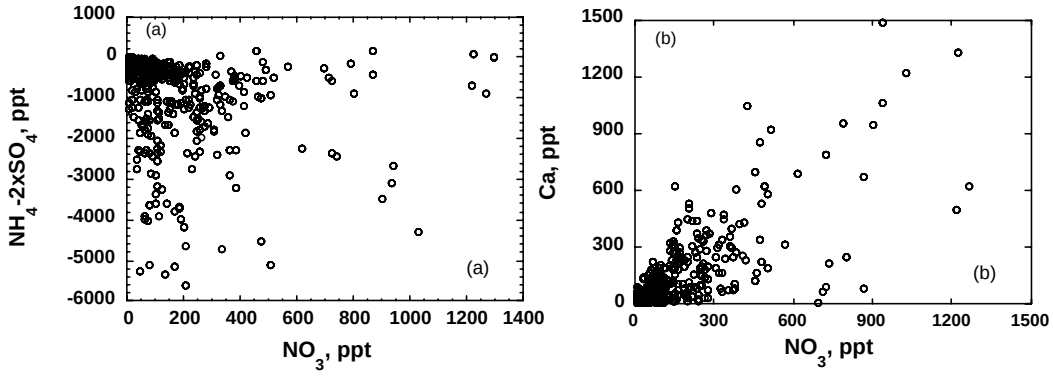

Figure 8 : Aerosol nitrate relationship with excess sulfate and calcium

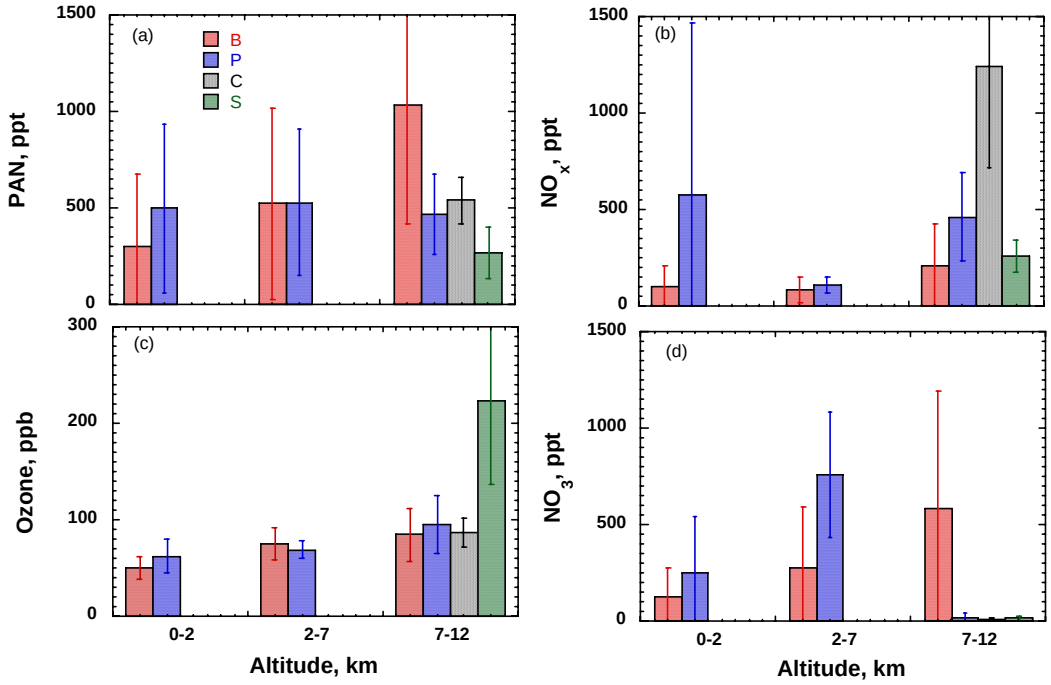

Figure 9: Distribution of selected chemicals in plumes of biomass combustion (B), anthropogenic pollution (P), convection (C), and stratosphere (S)

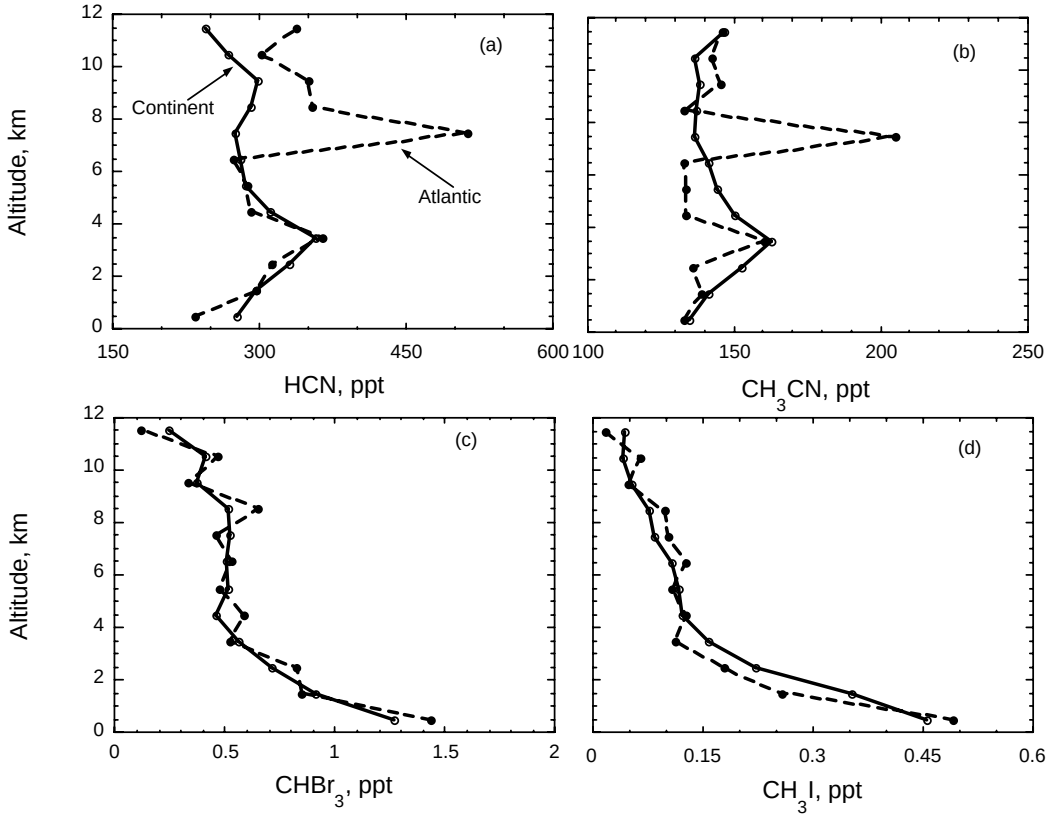

Figure 10: Vertical distribution of oceanic sourced tracers and nitriles.

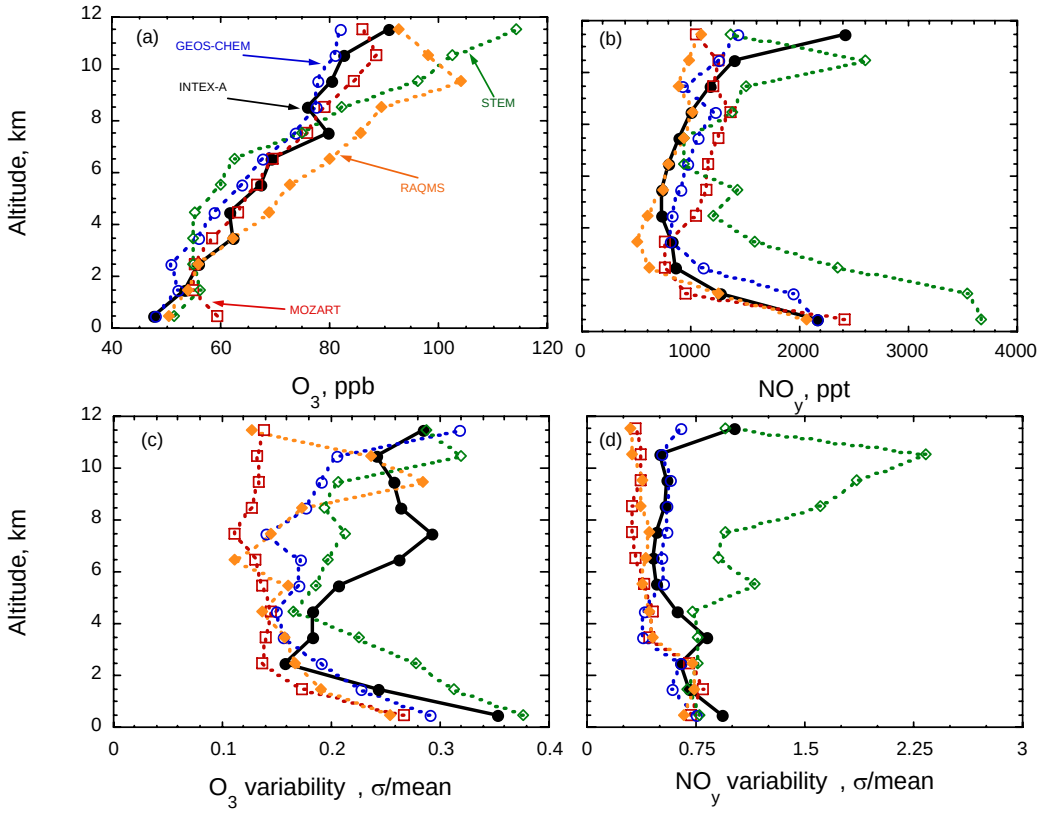

Figure 11: Observed and simulated mixing ratio and variability of O_3 and NO_y over eastern North America (30-50˚N; 260-320˚E). Top panels (a, b) -mean mixing ratios; Bottom panels (c, d) - relative variability

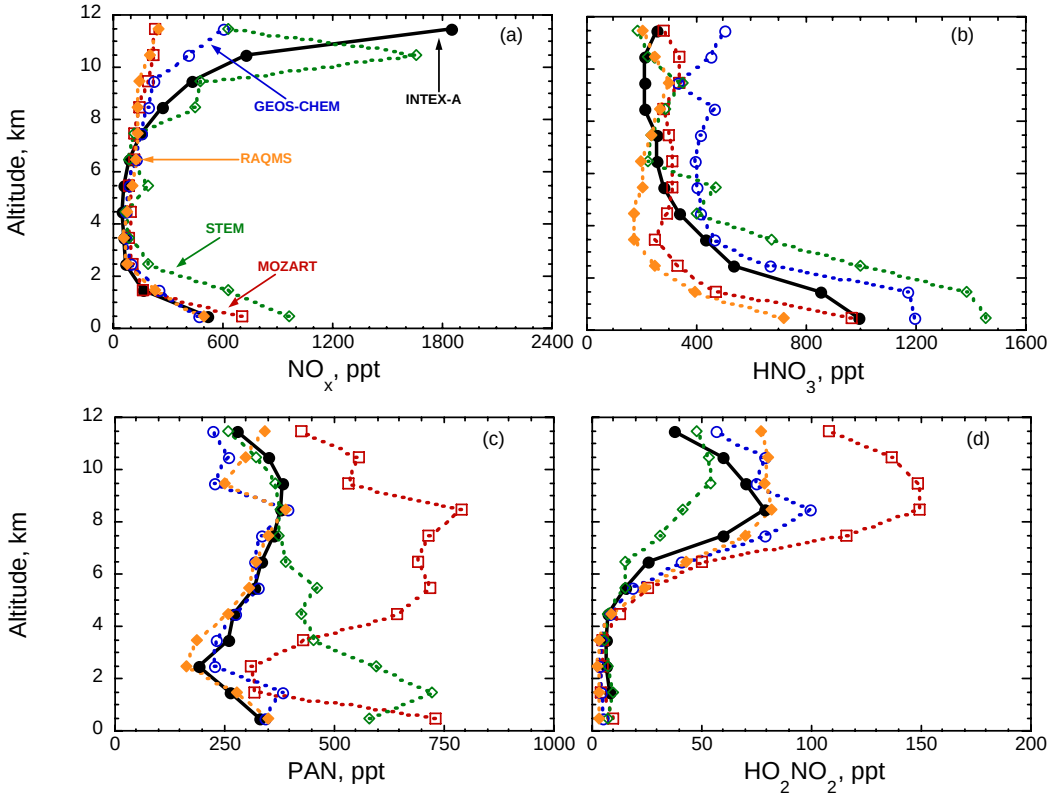

Figure 12: Observed and simulated mixing ratio of selected reactive nitrogen species over eastern North America (30-50˚N; 260-320˚E)

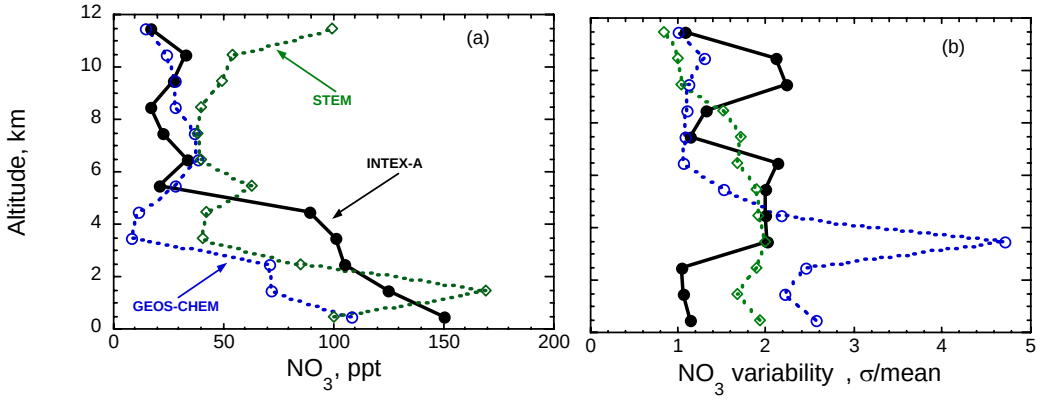

Figure 13: Observed and simulated aerosol nitrate concentrations and variability over eastern North America (30-50˚N; 260-320˚E). Aerosol size cut off is 2.5 μm.

Table 1: Reactive nitrogen, O_3, and CO mixing ratios in the North American troposphere during INTEX-A

Altitude (km)	O_3 (ppb)	CO (ppb)	NO_x (ppt)	HNO_3 (ppt)	PAN (ppt)	PPN (ppt)	HO_2NO_2 (ppt)	NO_3 (ppt)	NO_y (ppt)	$\sum RONO_2$ (ppt)	HCN (ppt)	CH_3CN (ppt)
0-2	48.9 ± 16.2 (48.4, 2607)*	132.1 ± 37.2 (127.4, 2079)	379 ± 823 (148, 1866)	893 ± 824 (701, 2467)	301 ± 339 (186, 1666)	32 ± 36 (20, 1666)	5 ± 8 (2, 78)	154 ± 183 (101, 1834)	1781 ± 1699 (1374, 1283)	18 ± 13 (15, 1473)	274 ± 76 (267, 1007)	136 ± 35 (132, 1007)
2-4	58.7 ± 11.8 (58.4, 1332)	112.7 ± 35.3 (107.6, 1107)	64 ± 63 (52, 975)	488 ± 358 (404, 1279)	214 ± 245 (158, 1021)	23 ± 26 (17, 1021)	10 ± 23 (2, 615)	110 ± 180 (34, 418)	809 ± 610 (652, 766)	11 ± 7 (9, 899)	337 ± 172 (310, 582)	153 ± 80 (138, 587)
4-6	63.3 ± 13.1 (62.6, 1268)	103.3 ± 26.7 (99.6, 1027)	54 ± 39 (47, 976)	317 ± 234 (269, 1216)	275 ± 228 (217, 981)	29 ± 24 (23, 981)	15 ± 31 (8, 1094)	90 ± 202 (10, 511)	733 ± 523 (613, 737)	9 ± 4 (8, 828)	296 ± 121 (285, 563)	144 ± 69 (136, 570)
6-8	72.4 ± 19.7 (71.3, 1492)	104.7 ± 51.8 (96.9, 1241)	113 ± 85 (92, 1154)	252 ± 185 (210, 1415)	354 ± 253 (298, 1106)	38 ± 27 (32, 1106)	41 ± 34 (31, 1353)	58 ± 202 (13, 786)	849 ± 511 (755, 856)	9 ± 5 (8, 907)	308 ± 258 (273, 630)	148 ± 97 (137, 667)
8-10	76.6 ± 20.2 (74.3, 1523)	102.3 ± 20.9 (101.3, 1175)	323 ± 288 (240, 1256)	202 ± 186 (146, 1497)	371 ± 217 (339, 1138)	39 ± 23 (36, 1138)	73 ± 40 (66, 1406)	27 ± 45 (11, 909)	1040 ± 570 (931, 923)	10 ± 6 (9, 954)	315 ± 138 (297, 595)	138 ± 40 (133, 720)
10-12	82.7 ± 20.5 (82.2, 942)	96.5 ± 22.8 (93.7, 687)	776 ± 900 (552, 700)	205 ± 153 (159, 901)	338 ± 208 (295, 650)	36 ± 22 (31, 650)	53 ± 30 (49, 868)	34 ± 60 (21, 818)	1430 ± 1052 (1197, 465)	8 ± 6 (7, 586)	274 ± 73 (284, 404)	141 ± 20 (141, 406)
0-12	64.2 ± 20.9 (62.9, 9164)	112.3 ± 37.8 (106.2, 7316)	275 ± 572 (106, 6927)	462 ± 558 (285, 8775)	308 ± 269 (246, 6562)	33 ± 28 (26, 6562)	42 ± 41 (29, 5414)	90 ± 167 (28, 5276)	1152 ± 1099 (829, 5030)	12 ± 9 (9, 5647)	299 ± 153 (285, 3781)	142 ± 63 (136, 3967)

* Mean ± sigma (Median, No. of points)

Table 2: Alkyl nitrate (C_1-C_5) mixing ratios in the North American troposphere during INTEX-A

Altitude (km)	CH_3ONO_2 (ppt)	$C_2H_5ONO_2$ (ppt)	i-$C_3H_8ONO_2$ (ppt)	n-$C_3H_8ONO_2$ (ppt)	2-$C_4H_{10}ONO_2$ (ppt)	3-$C_5H_{12}ONO_2$ (ppt)	2-$C_5H_{12}ONO_2$ (ppt)	$\sum RONO_2$ (ppt)	TANs** (ppt)
0-2	2.3 ± 0.7 (2.1, 1467) *	2.3 ± 1.1 (2.0, 1467)	5.4 ± 4.0 (4.4, 1467)	0.7 ± 0.5 (0.6, 1467)	4.6 ± 4.5 (3.5, 1467)	1.4 ± 1.4 (1.1, 1469)	1.8 ± 2.0 (1.3, 1473)	18 ± 13 (15, 1473)	191 ± 204 (147, 1713)
2-7	1.9 ± 0.4 (1.9, 2198)	1.5 ± 0.5 (1.5, 2198)	2.9 ± 1.7 (2.6, 2198)	0.3 ± 0.2 (0.3, 2198)	2.1 ± 2.0 (1.6, 2198)	0.5 ± 0.6 (0.3, 2214)	0.5 ± 0.7 (0.3, 2219)	10 ± 6 (9, 2219)	
7-12	2.1 ± 0.5 (2.1, 1890)	1.7 ± 0.7 (1.6, 1890)	3.7 ± 3.0 (2.9, 1890)	0.3 ± 0.2 (0.2, 1900)	1.5 ± 2.1 (0.7, 1894)	0.2 ± 0.5 (0.1, 1936)	0.1 ± 0.3 (0.03, 1950)	10 ± 6 (8, 1950)	

* Mean ± sigma (Median, No. of points)

** Total Alkyl Nitrates (TANs) were measured in the lower troposphere ($Z < 4$ km) by thermally dissociating these to NO_2 (see text).